

ORIGINAL
RESEARCH

P.H. Lai
H.H. Weng
C.Y. Chen
S.S. Hsu
S. Ding
C.W. Ko
J.H. Fu
H.L. Liang
K.H. Chen

In Vivo Differentiation of Aerobic Brain Abscesses and Necrotic Glioblastomas Multiforme Using Proton MR Spectroscopic Imaging

BACKGROUND AND PURPOSE: Abscesses caused by aerobic bacteria (aerobic abscesses) can simulate intracranial glioblastomas multiforme (GBMs) in MR imaging appearance and single voxel (SV) proton MR spectroscopy of the central cavity. The purpose of our study was to determine whether MR spectroscopic imaging (SI) can be used to differentiate aerobic abscesses from GBMs. Our hypothesis was that metabolite levels of choline (Cho) are decreased in the ring-enhancing portion of abscesses compared with GBMs.

MATERIALS AND METHODS: Fifteen patients with aerobic abscesses were studied on a 1.5T MR scanner using an SV method and an SI method. Proton MR spectra of 15 GBMs with similar conventional MR imaging appearances were used for comparison. The resonance peaks in the cavity, including lactate, cytosolic amino acids, acetate, succinate, and lipids, were analyzed by both SV MR spectroscopy and MRSI. In the contrast-enhancing rim of each lesion, peak areas of *N*-acetylaspartate (NAA), choline (Cho), lipid and lactate (LL), and creatine (Cr) were measured by MRSI. The peak areas of NAA-n, Cho-n, and Cr-n in the corresponding contralateral normal-appearing (-n) brain were also measured. Maximum Cho/Cr, Cho/NAA, LL/Cr-n, and Cho/Cho-n and minimum Cr/Cr-n and NAA/NAA-n ratios in abscesses and GBMs were compared using the Wilcoxon rank sum test. After receiver operating characteristic curve analysis, diagnostic accuracy was compared.

RESULTS: Cytosolic amino acid peaks were found in the cavity in 7 of 15 patients with aerobic abscesses. Means and SDs of maximum Cho/Cr, Cho/NAA, LL/Cr-n, and Cho/Cho-n and minimum Cr/Cr-n and NAA/NAA-n ratios were 3.38 ± 1.09 , 3.88 ± 2.13 , 2.72 ± 1.45 , 1.98 ± 0.53 , 0.53 ± 0.16 , and 0.44 ± 0.09 , respectively, in the GBMs, and 1.77 ± 0.49 , 1.48 ± 0.51 , 2.11 ± 0.67 , 0.81 ± 0.21 , 0.48 ± 0.2 , and 0.5 ± 0.15 , respectively, in the abscesses. Significant differences were found in the maximum Cho/Cr ($P = .001$), Cho/NAA ($P = .006$), and Cho/Cho-n ratios ($P < .001$) between abscesses and GBMs. Diagnostic accuracy was higher by Cho/Cho-n ratio than Cho/Cr and Cho/NAA ratios (93.3% versus 86.7% and 76.7%).

CONCLUSION: Metabolite ratios and maximum Cho/Cho-n, Cho/Cr, and Cho/NAA ratios of the contrast-enhancing rim were significantly different and useful in differentiating aerobic abscesses from GBMs by MRSI.

Brain abscess can be a lethal condition if appropriate treatment is delayed. Thus, early diagnosis of brain abscess is desired and is a challenge for clinicians and radiologists. Radiologically, a brain abscess in the capsule stage appears in CT and in MR imaging as an expansile, rim-enhancing mass surrounded by edema, which is similar in appearance to necrotic malignant tumors, especially glioblastoma multiforme

(GBM).^{1,2} Clinically, both brain abscesses and GBMs may cause nonspecific headaches in the absence of fever, focal neurologic deficits, epileptic seizures, and disturbances in higher-level cortical function. In addition, laboratory examination often shows normal white blood cell count.^{1,2} Further reduction of mortality from brain abscesses requires more rapid, accurate, and safe diagnostic techniques. Application of diffusion-weighted imaging (DWI) in distinguishing between pyogenic brain abscesses and cystic or necrotic brain tumors has been reported to be useful in many publications.³⁻⁸ The cystic or necrotic portion of tumors almost always has a low signal intensity on DWI and a higher apparent diffusion coefficient (ADC) value; however, some exceptions have been reported for necrotic brain tumors.⁷⁻¹² Hyperintensity with restricted diffusion is diagnostic, but not pathognomonic, for pyogenic abscess on DWI. However, exceptions of DWI studies and substantial variability in the ADCs have been reported for pyogenic abscesses.^{8,12-16}

Single-voxel proton MR spectroscopy of the central cystic portion has been reported to allow the broad group of pyogenic abscesses to be distinguished from malignant gliomas.¹⁷⁻²² Acetate, succinate, and amino acids have been identified in cerebral abscesses in humans and were used as

Received February 6, 2008; accepted after revision March 13.

From the Departments of Radiology (P.H.L., J.H.F., H.L.L., K.H.C.) and Neurosurgery (S.S.H.), Veterans' General Hospital, Kaohsiung, and School of Medicine, National Yang-Ming University, Taipei, Taiwan, Republic of China; Department of Radiology (H.H.W.), Chang Gung Memorial Hospital-Chiayi, Chang Gung University College of Medicine, and Graduate Institute of Occupational Safety and Health, College of Health Sciences, Kaohsiung Medical University, Kaohsiung, Taiwan, Republic of China; Department of Radiology (C.Y.C.), Chi Mei Hospital, Taiwan, Republic of China; Departments of Chemistry (S.D.) and Computer Science and Engineering (C.W.K.), National Sun Yat-Sen University, Taiwan, Taiwan, Republic of China.

This work was supported in parts by grants from the National Science Council (NSC-94-2314-B-075B-008 and NSC-95-2314-B-075B-009 to P.H.L.) and Veterans' General Hospital Kaohsiung (VGHKS 96-061 and VGHKS 97-056 to P.H.L.) and Veterans' General Hospital National Sun Yat-Sen University (VGHNSU-94-007 to P.H.L.).

Please address correspondence to Ping-Hong Lai, Faculty of National Yang-Ming University School of Medicine, Department of Radiology, Veterans' General Hospital-Kaohsiung, 386 Ta-Chung First Rd, Kaohsiung, Taiwan 813, Republic of China; e-mail: phlai@vghks.gov.tw

DOI 10.3174/ajnr.A1130

bacterial marker metabolites for noninvasive diagnosis by MR spectroscopy.¹⁷⁻²² Abscesses caused by anaerobic bacteria have been distinguished from those caused by aerobic bacteria based on metabolites detectable with MR spectroscopy (acetate and succinate).²¹⁻²³ However, spectral patterns recorded for the cystic or necrotic components of GBMs and abscesses caused by aerobic bacteria (aerobic abscesses) were similar by single-voxel MR spectroscopy.^{18,21,24} Diagnosis based on such subjectively selected metabolites or metabolite ratios was not possible.²⁴

At pathologic examination, the enhancing rim of GBMs represents infiltrating tumor cells,^{25,26} and an increased Cho/Cr ratio was observed. Pathologically, the enhancing rim of a pyogenic abscess represents an inflammatory infiltrate composed of neutrophils and, later, macrophages and lymphocytes. Granulation tissue surrounds the area of inflammation and eventually develops into a fibrous capsule. This capsule, in turn, is surrounded by gliotic, edematous brain tissue. In the experimental setting, brain abscesses have been shown to have relatively high amounts of mature collagen and decreased neovascularity.^{27,28} The Cho/Cr ratio of rim-enhancing lesion of abscesses would be presumed to be less than that of GBMs.

Recent developments in MR spectroscopy have made it possible to obtain spectroscopic MR imaging with high spatial resolution and multiple spectra simultaneously from contiguous voxels.^{29,30} To date, proton MR spectroscopic imaging has not been used to differentiate aerobic abscesses from GBMs. We aimed to test the feasibility of MR spectroscopic imaging to distinguish between aerobic abscesses and GBMs by the evaluation of the contrast-enhancing rim of the lesions. Our hypothesis was that metabolite levels of Cho are decreased in the rim-enhancing portion of aerobic abscesses relative to the Cho seen in the rim-enhancing portion of necrotic GBMs.

Materials and Methods

Patients

In this retrospective study between January 2001 and December 2006, a total of 56 consecutive patients with pyogenic brain abscesses were examined with *in vivo* MR spectroscopy. Adapted selection criteria from Himmelreich et al²⁴ were as follows: 1) a heavy, pure growth of obligate or facultative aerobic bacteria was observed from pus obtained within 2 days of the MR examination; 2) patients had not received antibiotics for longer than 2 days at the time of the MR examination; and 3) abscesses were at least 2 cm in diameter to place the volume of interest (VOI) in the center of the abscess with minimal "contamination" from surrounding brain tissue by MR spectroscopy. Sixteen patients met the above selection criteria, and the spectrum of 1 patient was obtained in poor quality due to movement artifacts. Therefore, 15 patients with obligate or facultative aerobic bacteria brain abscesses were included in the study.

For comparison, we selected 15 patients with GBMs (≥ 2 cm in diameter) that had similar conventional MR imaging features, that is, perilesion contrast enhancement with gadolinium chelates. All of the GBMs were diagnosed by histopathologic examination after either stereotactic biopsy (in 3 patients) or surgical resection (in 2 patients). Approval for this study was obtained from our institutional review board, and informed consent was obtained from all of the patients.

Proton MR Spectroscopy Methods

Single Voxel Spectroscopy. All of the proton MR spectroscopy examinations were performed on a 1.5T scanner (Signa; GE Medical System, Milwaukee, Wis). The selection of voxel position in the estimated center of the lesion was determined visually by examining the MR images in 3 orthogonal planes (sagittal, coronal, and axial) to define a $1.5 \times 1.5 \times 1.5 \times 2 \times 2 \times 2$ cm VOI. Single-voxel spectroscopy was applied by using the method of the point-resolved spectroscopy sequence (PRESS). After automated transmitter and receiver adjustment, the signal intensity over the VOI was shimmed to within a typical full width at a half maximum (FWHM) of 4–8 Hz in all of the examinations. Optimal water resonance suppression was achieved by preirradiation of the water resonance with 3 chemical shift selective pulse sequences and spoiled gradient pulses. The parameters used were a TR of 1600 ms, TE of both 272 ms and 136 ms, 192 acquisitions, a spectral width of 2500 Hz, and 2048 data points in all of the patients. A TE of 136 ms was used to confirm the phase inversion associated with J-coupled metabolites of lactate (1.3 ppm) and cytosolic amino acids (0.9 ppm) but not of lipids, which may be helpful in discriminating lactate or amino acid signals from lipid signals.¹⁷⁻²² The acquisition time for each sequence was 5 minutes and 45 seconds. The MR spectroscopy data files were transferred to an off-line workstation for postprocessing by 2 experienced neuroradiologists independently by using FuncTool software (GE Medical Systems). Direct current correction, zero-filling to 4096 data points, 1.0-Hz exponential apodization, Fourier transformation, and zero-order phase were carried out for further peak assignment based on the literature.¹⁷⁻²²

MR Spectroscopic Imaging. Spectroscopic imaging was conducted with a PRESS sequence. The following parameters were used: TR/TE, 1500/136 ms; acquisition, 2 averages; and acquisition time, 12 minutes 55 seconds. A typical VOI consists of an 80- × 80-mm region placed within a 160- × 160-mm FOV on a 10- to 15-mm transverse section. A 16×16 phase-encoding matrix was used to obtain the 8×8 array of spectra in the VOI with an in-plane resolution of 10×10 mm and a voxel size of $1 \times 1 \times 1$ cm or $1 \times 1 \times 1.5$ cm, depending on the size of the lesion. The VOI was determined by contrast-enhanced axial T1-weighted as well as fluid-attenuated inversion recovery (FLAIR) images simultaneously to ensure that voxels were placed with certainty both over the contrast-enhancing area and contralateral normal-appearing brain tissue, which was defined as not displaying signal intensity alterations on FLAIR imaging. To avoid contamination from scalp fat, the VOI was completely enclosed within the brain and positioned at the center of the phase-encoded FOV. Automatic prescanning was performed twice before each spectroscopic scan to ensure adequate water suppression. The FWHM was kept under 10 Hz. The resonance peaks in the cavity, including lactate at 1.3 ppm, cytosolic amino acids (leucine, isoleucine, and valine) at 0.9 ppm, alanine at 1.50 ppm, acetate at 1.92 ppm, succinate at 2.4 ppm, and lipids (0.8–1.3 ppm) were analyzed in all of the patients by both single-voxel MR spectroscopy and MR spectroscopic imaging.

Spectra were processed by 2 experienced neuroradiologists independently by using an off-line workstation with FuncTool software (GE Medical Systems). The signal intensity of various metabolite peaks was evaluated in every voxel by using the integral of each peak as a measure of its intensity. In the contrast-enhancing rim of each lesion, we estimated the peak areas of Cho compounds at 3.21 ppm, CR phosphocreatine at 3.04 ppm, and *N*-acetylaspartate (NAA) at 2.02 ppm. Lipid (Lip) and lactate (Lac), at intermediate TE (136 ms) were estimated by using the sum of the upright Lip peak around 0.9–1.3 ppm and the absolute value of the inverted Lac peak at 1.3 ppm due to

Table 1: MR spectroscopy metabolite ratios of GBMs and aerobic abscesses

Variable	Maximum Cho/Cr	Maximum Cho/NAA	Maximum LL/Cr-n	Maximum Cho/Cho-n	Minimum Cr/Cr-n	Minimum NAA/NAA-n	Cho-n/Cr-n	Cho-n/NAA-n
GBM	3.38 ± 1.09	3.88 ± 2.13	2.72 ± 1.45	1.98 ± 0.53	0.53 ± 0.16	0.44 ± 0.09	1.01 ± 0.11	0.74 ± 0.14
Abscess	1.77 ± 0.49	1.48 ± 0.51	2.11 ± 0.67	0.81 ± 0.21	0.48 ± 0.2	0.5 ± 0.15	0.98 ± 0.15	0.72 ± 0.13
<i>P</i>	.001	.006	NS (.198)	<.001	NS (.451)	NS (.387)	NS (.614)	NS (.728)

Note:—Cho indicates choline; Cr, creatine; NAA, *N*-acetylaspartate; LL, lipid and lactate; -n, normal; NS, not significant; GBM, glioblastoma multiforme.

the J modulation as a Lac/Lip (LL) mixture. We also measured the peak areas of NAA, Cho, and Cr in the corresponding contralateral normal-appearing white matter (if the lesion was located in either the cerebral hemispheric white matter) or corresponding contralateral normal-appearing deep gray matter (if the lesion was located in the basal ganglion or thalamus) as Cho-n, Cr-n, and NAA-n in each patient. Thus, each patient served as his or her own control. We used 3 spectra to derive the mean values for Cho-n, Cr-n, and NAA-n, and normal ratios for Cho-n/Cr-n and Cho-n/NAA-n were obtained. Metabolite ratios in the multiple voxels of the contrast-enhancing rim of each lesion were calculated for Cho/Cr, Cho/NAA, LL/Cr-n, Cho/Cho-n, Cr/Cr-n, and NAA/NAA-n ratios. The voxel number was dependent on the lesion size (2.5–5.5 cm in diameter) and ranged between 7 and 23. The maximum Cho/Cr, Cho/NAA, LL/Cr-n, Cho/Cho-n ratios and minimum Cr/Cr-n and NAA/NAA-n ratios were used for comparison among the GBMs and abscesses.

Statistical Analysis

The data were summarized by using the mean and SD. A nonparametric test for nonnormalized paired data, a Wilcoxon signed-rank test, was used to compare the maximum Cho/Cr and Cho/NAA ratios in each region of the abscesses or GBMs with Cho-n/Cr-n and Cho-n/NAA-n of the contralateral normal-appearing brain. A nonparametric test for independent samples, a Wilcoxon rank sum test, was used to compare maximum Cho/Cr, Cho/NAA, LL/Cr-n, and Cho/Cho-n ratios and minimum Cr/Cr-n and NAA/NAA-n ratios between corresponding rim-enhancing regions of abscesses and GBMs (eg, to compare the maximum Cho/Cr ratio in the rim-enhancing region of abscesses with the maximum Cho/Cr ratio in the rim-enhancing region of GBMs). All of the statistical analyses were performed by using STATA software (version 9.2; Stata, College Station, Tex). A *P* value less than .05 was considered to indicate a significant difference.

Receiver operating characteristic (ROC) curve analysis was done to evaluate the performance of the maximum Cho/Cr, Cho/NAA, and Cho/Cho-n ratios in differentiating GBMs from aerobic abscesses by using the ROCKIT algorithm (available through the Internet from C. E. Metz, University of Chicago, http://xray.bsd.uchicago.edu/krl/roc_soft.htm). The area under the ROC curve (A_z) was calculated to summarize the performance of each maximum Cho/Cr, Cho/NAA, and Cho/Cho-n ratio in the task of differentiation. We calculated sensitivity, specificity, positive predictive value (PPV), and negative predictive value (NPV) by using maximum Cho/Cr, Cho/NAA, and Cho/Cho-n ratios of the cutoff value obtained with minimum C1 error from the ROC analysis, where $C1 = 1 - (\text{sensitivity} + \text{specificity})/2$. When any ratio of maximum Cho/Cho-n or maximum Cho/Cr or maximum Cho/NAA was larger than its cutoff value, we regarded it as a GBM. Afterward, diagnostic accuracy, sensitivity, specificity, PPV, and NPV, including 95% confidence interval (CI), were also calculated and compared.

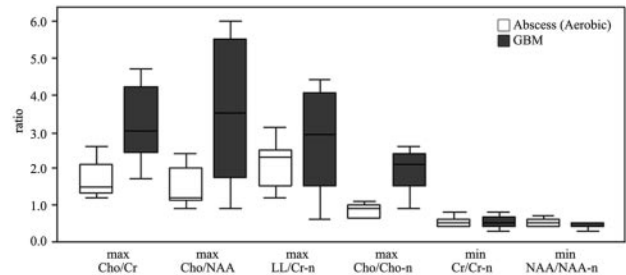


Fig 1. Box plots of the ratios of the metabolites in patients with aerobic abscesses (white box) and GBMs (gray box). The middle horizontal line is the median, the upper and lower ends of the boxes are the third and first quartiles, and the vertical lines show the full range of values in the data. max indicates maximum; min, minimum.

Results

Fifteen patients had obligate or facultative aerobic bacteria (6 *Pseudomonas aeruginosa*, 3 *Streptococcus intermedius*, and 6 *Staphylococcus aureus*) brain abscesses, and these patients included 8 men and 7 women with an age range of 30–80 years and a mean age of 61.8 years. Fifteen patients with GBMs included 7 men and 8 women with an age range of 43–79 years and a mean age of 62.2 years.

The predominant resonance lines NAA, Cho, and Cr that are usually observed in the parenchyma of the normal brain were hardly detectable in the central necrotic fluid of the abscesses and GBMs. In vivo proton MR spectroscopy single voxel spectra in 10 of 15 patients with a cystic or necrotic tumor showed only the peak attributed to lactate. Lactate and lipid were found in 5 patients with a tumor. Single-voxel spectra in 7 of 15 patients with aerobic abscesses showed lactate and cytosolic amino acids. Lactate and lipid were found in 8 patients with aerobic abscesses. No resonances arising from acetate and succinate were detected, in contrast to spectra from mixed anaerobic bacterial abscesses. MR spectroscopic imaging showed the above similar findings in the central cavity of the abscesses and GBMs compared with single-voxel MR spectroscopy.

MR spectroscopic imaging measured metabolite ratios of the contrast-enhancing rim of GBMs, and aerobic abscesses are summarized in Table 1 and Fig 1. Means of maximum Cho/Cr, Cho/NAA, LL/Cr-n, and Cho/Cho-n and minimum Cr/Cr-n and NAA/NAA-n ratios were 3.38 ± 1.09, 3.88 ± 2.13, 2.72 ± 1.45, 1.98 ± 0.53, 0.53 ± 0.16, and 0.44 ± 0.09, respectively, in the GBMs and 1.77 ± 0.49, 1.48 ± 0.51, 2.11 ± 0.67, 0.81 ± 0.21, 0.48 ± 0.2, and 0.5 ± 0.15, respectively, in the aerobic abscesses. Significant differences were found in the maximum Cho/Cr (*P* = .001), Cho/NAA (*P* = .006), and Cho/Cho-n ratios (*P* < .001) between abscesses and GBMs. No significant differences were found in the maximum LL/Cr-n and minimum Cr/Cr-n and NAA/NAA-n ratios.

In GBMs, the maximum Cho/Cr and Cho/NAA were

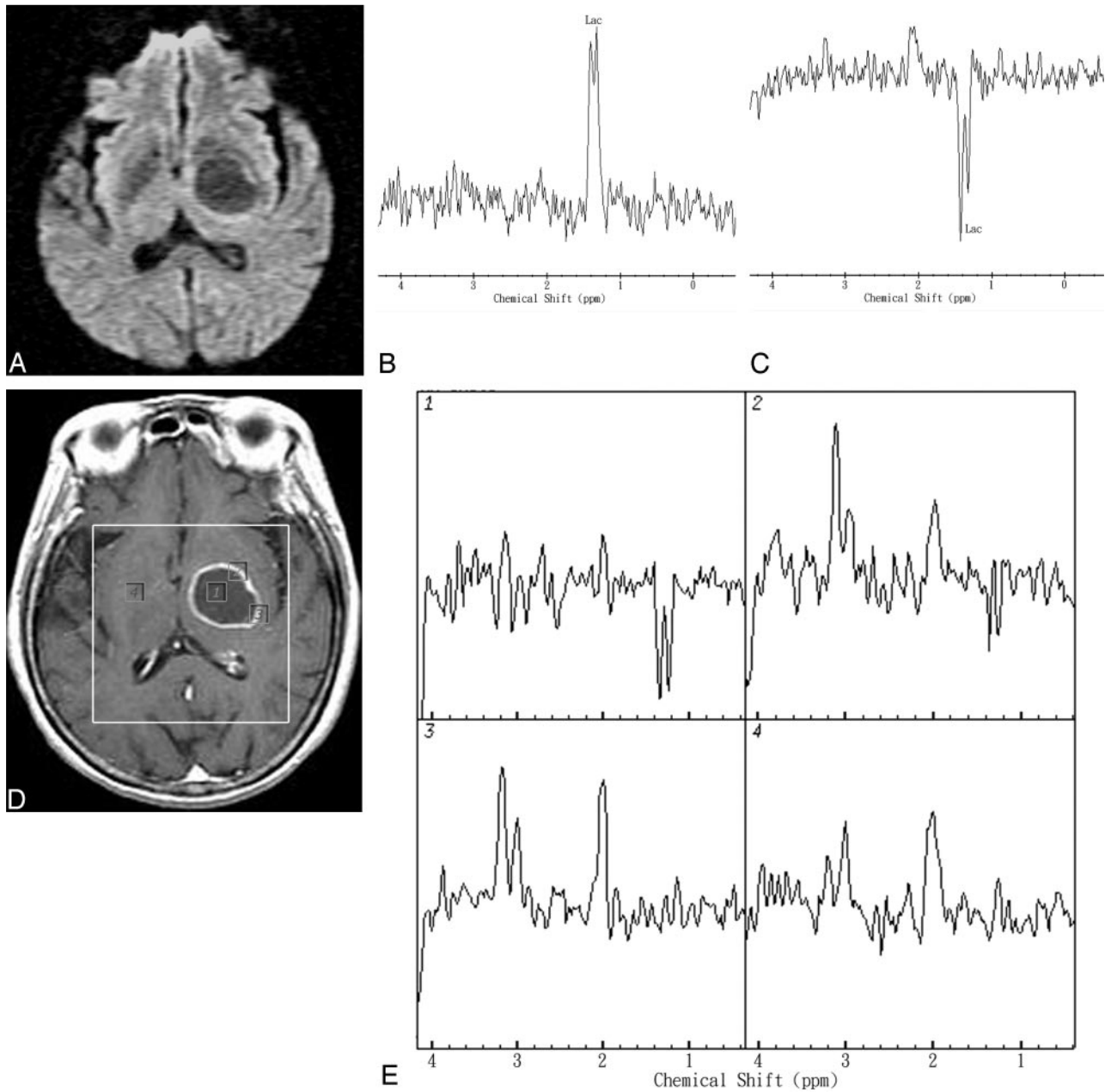


Fig 2. Representative in vivo MR images and spectra from a 67-year-old man with a pathologically proved left thalamus region GBM. *A*, DWI revealed hypointensity and increased ADC values in the range of $2.51\text{--}2.65 \times 10^{-3} \text{ mm}^2/\text{s}$ in the cavity of the mass lesion. *B* and *C*, In vivo proton single-voxel spectra with a point-resolved spectroscopy sequence (1600/272 ms and 136 ms) from the VOI centered within the cystic mass lesion show a Lac peak at 1.3 ppm that is inverted at a TE of 136 ms. *D*, Axial contrast-enhanced T1-weighted MR image (500/30) shows a ring-enhanced lesion in left thalamus region and the area of the spectroscopy measurement (VOI) on MR spectroscopic imaging. Voxels corresponding with the center and enhancing rim of the lesion and corresponding contralateral normal-appearing deep gray matter are highlighted in the contrast-enhanced T1-weighted MR image. The spectra were acquired with TE = 136 ms and nominal spatial resolution at 1 mL. *E*, The spectra from those voxels are shown in detail. The spectra show Lac peak in the center, increased Cho/Cr ratio (maximum, 2.43), and increased Cho/Cho-n ratio (maximum, 2.54) in the rim-enhancing areas of the mass lesion. The contralateral normal-appearing deep brain region does not show any spectral alterations.

significantly elevated compared with contralateral normal-appearing brain ($P < .001$). Spectra of the enhancing rim of GBMs typically show a decreased NAA level, an increased Cho/Cr ratio, and elevated Lac/Lip signals. The enhancing rim of GBMs revealed an increased level of Cho and decreased levels of Cr and NAA in comparison with the normal contralateral brain. One representative case that illustrates the diagnostic use of the MR spectroscopic imaging of the GBM is shown in Fig 2. A 67-year-old man complained of headache and presented with right hemiparesis. MR im-

aging showed a ring-enhanced mass lesion in the left thalamus region. DWI revealed hypointensity and increased ADC values in the range of $2.51\text{--}2.65 \times 10^{-3} \text{ mm}^2/\text{s}$ in the cavity of the mass lesion. Single-voxel MR spectroscopy showed a Lac peak within the center of the lesion. MR spectroscopic imaging revealed a Lac peak in the center, increased Cho/Cr ratio (maximum, 2.43), and increased Cho/Cho-n ratio (maximum, 2.54) in the rim-enhancing areas of the mass lesion compared with the corresponding contralateral normal-appearing brain region (Cho-n/Cr-n,

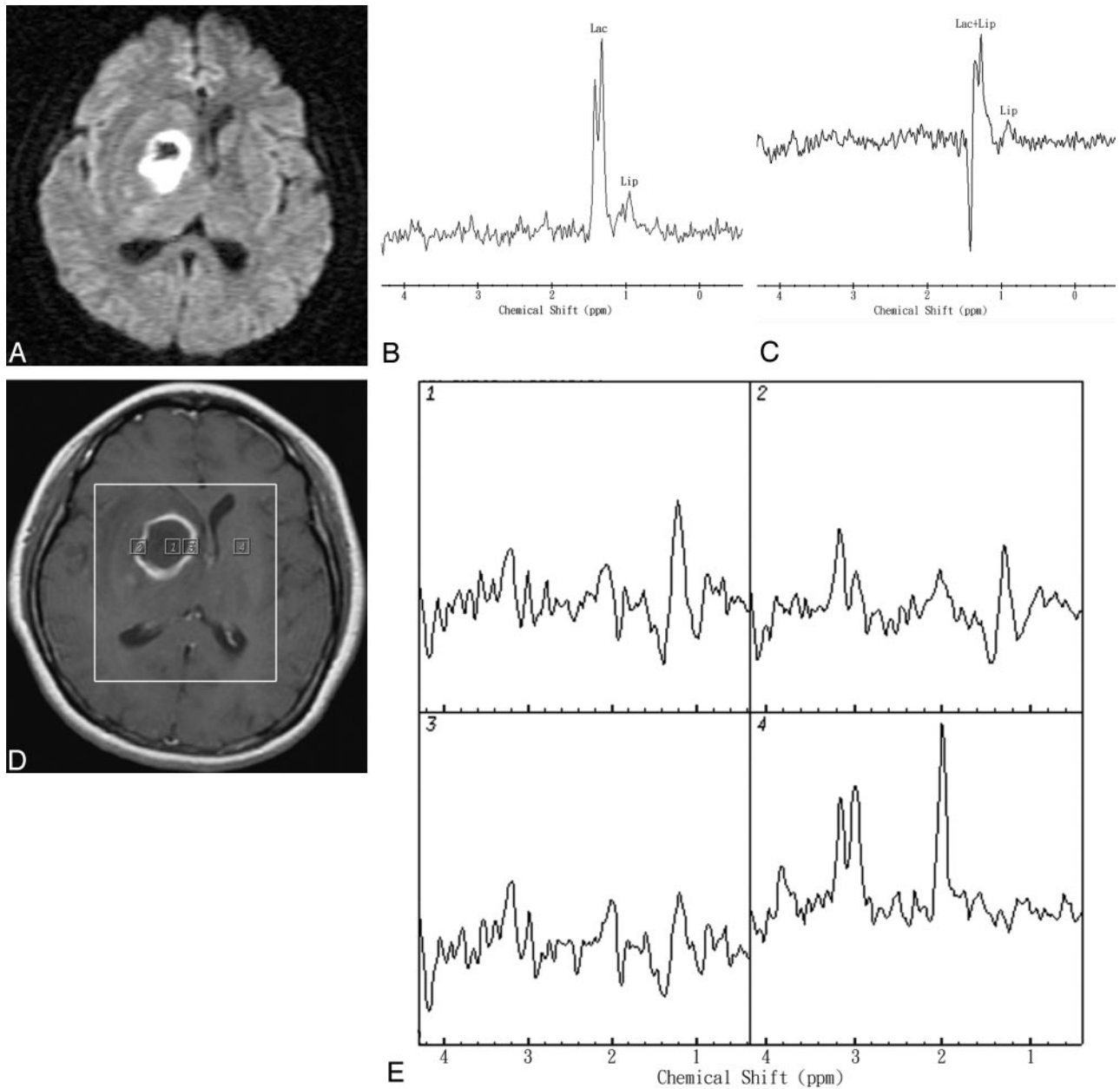


Fig 3. Representative in vivo MR images and spectra from a 65-year-old woman with stereotactic aspiration proved pyogenic brain abscess in the right deep basal ganglion region secondary to *S aureus* (facultative aerobic) infection. *A*, DWI revealed heterogeneous hyperintensity and reduced ADC values in the range of $0.48\text{--}0.71 \times 10^{-3} \text{ mm}^2/\text{s}$ in most of the cavity. *B* and *C*, In vivo proton single-voxel spectra with point-resolved spectroscopy sequence (1600/272 ms and 136 ms) from the VOI centered within the cystic mass lesion show Lac signal intensity at 1.3 ppm, which is inverted at a TE of 136 ms and Lip signal intensity at 0.9–1.3 ppm. *D*, Axial contrast-enhanced T1-weighted MR image (500/30) shows a rim-enhanced lesion in the right basal ganglion region and the area of the spectroscopy measurement (VOI) on MR spectroscopic imaging. Voxels corresponding with the center and enhancing rim of the lesion and corresponding contralateral normal-appearing deep gray matter are highlighted in the contrast-enhanced T1-weighted MR image. *E*, The spectra from those voxels are shown in detail. The spectra show Lac and Lip peaks in the center, mild increased Cho/Cr ratio (maximum, 1.82), and decreased Cho/Cho-n ratio (maximum, 0.85) in the rim-enhancing areas of the mass lesion. The contralateral normal-appearing deep brain region does not show any spectral alterations.

1.09). Stereotactic biopsy was performed and histologic study demonstrated GBM.

In abscesses, the maximum Cho/Cr and Cho/NAA were significantly elevated compared with contralateral normal-appearing brain ($P = .001$). Spectra of the enhancing rim of a pyogenic abscess typically show mildly increased Cho/Cr and Cho/NAA ratios and elevated Lac. The enhancing rim of abscesses showed a normal-to-mild decreased Cho level and decreased levels of Cr and NAA in comparison with normal contralateral brain. The Cho/Cr ratio is lower than that often seen in GBMs ($P = .001$), though 2 tumors have a Cho/Cr ratio

similar to abscesses. The Cho levels of rim-enhancing regions of abscesses were significantly lower than those of the rim-enhancing GBMs ($P < .001$). One representative case that illustrates the diagnostic use of the MR spectroscopic imaging of the aerobic abscess is shown in Fig 3. A 65-year-old woman presented with left hemiparesis. She had no fever or inflammatory signs. MR imaging showed a ring-enhanced mass lesion in the right deep basal ganglion region. DWI revealed heterogeneous hyperintensity and reduced ADC values in the range of $0.48\text{--}0.71 \times 10^{-3} \text{ mm}^2/\text{s}$ in most of the cavity. Single-voxel MR spectroscopy showed Lac and Lip peaks within

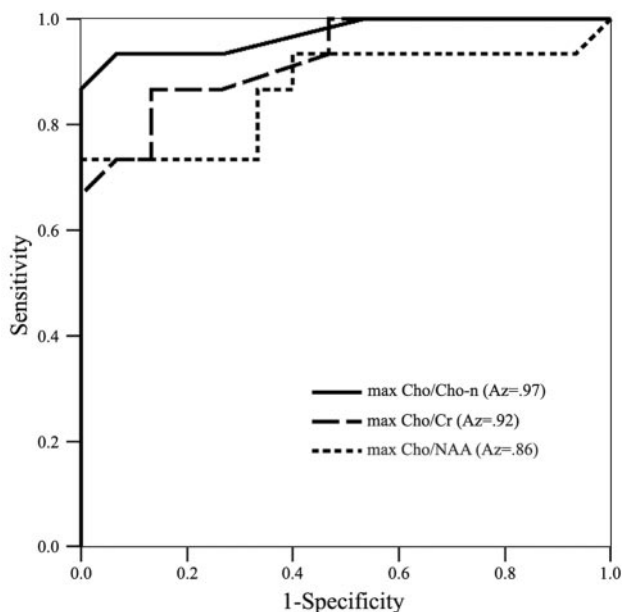


Fig 4. Graph shows 3 ROC curves of maximum (max) Cho/Cho-n, maximum (max) Cho/Cr, and maximum (max) Cho/NAA ratios for differentiation of GBMs from aerobic abscesses. A_z value area under the ROC curve is the highest (0.97) in the maximum Cho/Cho-n ratio and lowest (0.86) in the maximum Cho/NAA ratio.

the center of the lesion. MR spectroscopic imaging revealed Lac and Lip peaks in the center, a mild increased Cho/Cr ratio (maximum, 1.82), and decreased Cho/Cho-n ratio (maximum, 0.85) in the rim-enhancing areas of the mass lesion compared with the corresponding contralateral normal-appearing brain region (Cho-n/Cr-n, 1.03). Stereotactic aspiration surgery revealed an abscess with a positive-culture of *S aureus* (facultative aerobe).

In the evaluation of the performance differences of maximum Cho/Cr, Cho/NAA, and Cho/Cho-n ratios in the differentiation between GBMs and aerobic abscesses by using ROC analysis, the corresponding ROC curves and the A_z values for each metabolite ratio are shown in Fig 4. A_z value area under the ROC curve is the highest (0.97) in the maximum Cho/Cho-n ratio and lowest (0.86) in the maximum Cho/NAA ratio. Cutoff values with a minimum CI error of maximum Cho/Cho-n, Cho/Cr, and Cho/NAA were 1.05, 2.31, and 1.65, respectively. Diagnostic accuracy, sensitivity, specificity, PPV, and NPV, including 95% CIs of maximum Cho/Cho-n, Cho/Cr, and Cho/NAA ratios for differentiating GBMs from abscesses, are given in Table 2. Diagnostic accuracy was higher by maximum Cho/Cho-n ratio than by maximum Cho/Cr and Cho/NAA ratios (93.3% versus 86.7% and 76.7%).

Discussion

It may be possible to differentiate anaerobic brain abscesses from other pyogenic (ie, aerobic or sterile) brain abscesses on the basis of metabolite patterns seen at in vivo proton MR spectroscopy.²¹⁻²⁴ Typical features of MR spectra from anaerobic bacterial abscesses, such as succinate or acetate or increased amino acid resonances, were not detectable in *Staphylococcal aureus* (facultative aerobic bacteria) abscesses in rats or humans.^{17,18,21-24} Acetate, which is often referred to as a “marker” metabolite for in vivo diagnosis of bacterial abscesses at MR spectroscopy,¹⁷⁻²² was usually absent in aerobic

bacteria abscesses. Thus, interpretation of in vivo MR spectra by resonance assignment could allow us to distinguish between abscesses due to aerobic bacteria and those where anaerobic bacteria are present. However, the cystic components of the spectra in GBMs and abscesses by aerobes microorganisms would be similar by demonstration of Lip and/or Lac. Although MR spectroscopic findings from pus of staphylococcal abscesses and central necrotic fluid of GBMs in an animal model were distinguished by statistical classification strategy with an accuracy of 99%, the results are not directly translatable to in vivo diagnosis in humans.²⁴

Evaluation of cystic and rim-enhancing parts of lesions and normal parenchyma is more advantageous with multivoxel techniques. Multivoxel spectroscopy, MR spectroscopic imaging, or chemical-shift imaging acquires spectroscopic information from a large VOI in a single measurement. MR spectroscopic imaging can be combined with conventional MR imaging, because spectral patterns and metabolite concentrations can be overlaid on gray-scale imaging to compare voxels containing normal parenchyma and voxels containing pathology and also to obtain distributional patterns of specific metabolites.^{29,30} The information provided can, as illustrated in Figs 2 and 3, be used for the differential diagnosis of rim-enhancing GBMs versus aerobic abscesses.

Spectra of the enhancing rim of the pyogenic abscess typically show a decreased NAA level, a decreased Cr level, no change to a mild decreased Cho level (no change to mild decrease in Cho/Cho-n), a mild elevated Cho/Cr ratio, and elevated Lac/Lip, in general agreement with a few published reports.^{17,31} These visible small resonances of Cho, Cr, and NAA of the enhancing rim of the abscesses were interpreted to be caused by partial volume effects, a combination of the resonances representing the cystic components and surrounding contrast-enhancing tissue. NAA is reduced due to loss of intact neuronal cells, and Cr is particularly diminished because of general breakdown of energy metabolism.

Based on our observations, we presume that the mild increased Cho/Cr ratio in abscesses is secondary to a more pronounced reduction of Cr than of Cho but not because of an elevation of Cho. This finding underscores the value of directly comparing abnormal with normal metabolite levels. In addition, the measurement of Cho/Cho-n and Cr/Cr-n ratios may increase the specificity in characterizing mass lesions in the clinical setting when absolute quantification cannot be made relative to an external standard. The Cho/Cho-n ratio (relative signal intensity) is superior to the Cho/Cr ratio, because the absolute change in metabolites is a more sensitive indicator compared with the “internal standard” of a mirror-image healthy brain. Regional and individual variability in Cr concentrations is known, and relative signal intensity or absolute metabolite quantification may increase the sensitivity and specificity of MR spectroscopy.³² Diagnostic accuracy was higher by Cho/Cho-n ratio than by Cho/Cr and Cho/NAA ratios in our study.

Signal intensities from the NAA and the Cr resonance lines are usually lower in the brain tumors than in the healthy brain tissue,^{25,33-35} whereas the Cho resonance line very often exhibits higher with respect to normal brain tissue, particularly at the tumor rim.^{25,33} In accordance with several other studies,^{25,33-35} we observed increased Cho, decreased NAA and Cr

Table 2: Diagnostic accuracies of metabolite ratios in differentiation of glioblastomas multiforme from aerobic abscesses

Variable	Accuracy, %	Sensitivity, %	Specificity, %	PPV, %	NPV, %
Max Cho/Cho-n \geq 1.05	93.3 (76.5–98.8)	93.3 (66.0–99.7)	93.3 (66.0–99.7)	93.3 (66.0–99.7)	93.3 (66.0–99.7)
Max Cho/Cr \geq 2.31	86.7 (68.4–95.6)	86.7 (58.4–97.7)	86.7 (58.4–97.7)	86.7 (58.4–97.7)	86.7 (58.4–97.7)
Max Cho/NAA \geq 1.65	76.7 (57.3–89.4)	86.7 (58.4–97.7)	66.7 (38.7–87.0)	72.2 (46.4–89.3)	83.9 (57.7–95.6)

Note:—Cho indicates choline; Cr, creatine; NAA, *N*-acetylaspartate; -n, normal; PPV, positive predictive value; NPV, negative predictive value; max, maximum. The 95% confidence interval is in parenthesis.

resonances, and an increased Cho/Cho-n ratio as common features of contrast-enhancing parts of a primary high-grade tumor. Contrast-enhancing parts of nonneoplastic brain abscess, on the other hand, showed decreased NAA, Cr, and Cho resonances and a decreased Cho/Cho-n ratio.

In proton MR spectroscopy, an elevation in Cho may be due to cell membrane synthesis, destruction, or both. Measurable levels of Cho vary considerably, depending on the cellular attenuation, tumor grade, and presence or absence of necrosis.^{25,33–35} Cho resonance is most prominent in regions with high neoplastic cellular attenuation and is progressively lower in moderate- and low-grade tumors.^{33–35} Immunohistologic markers of proliferative activity in gliomas and Ki-67 labeling and MIB-1 labeling indices have a strong linear correlation with Cho levels. Semiquantitative Cho values may be reliable imaging indicators of proliferation in gliomas.^{36,37} Paradoxically, some GBMs contain less Cho than normal brain tissue (lower Cho/Cr and Cho/NAA ratios), an effect of dilution of absolute cellular attenuation by the presence of extensive necrosis.^{33,34}

The finding of a single Lac peak and/or Lip peak in aerobic abscess and necrotic GBMs is nonspecific. It is not easy to differentiate lactate signals from lipid signals in clinical settings, and in many previous studies, Lac and Lip peaks were often combined and described as “Lac/Lip mixture.”^{34,35} Lip signals are characteristic of high-grade tumors at short TE^{33,34} but are only observed in 41% of high-grade tumors at long TE³⁸ due to the much shorter T2 relaxation times of Lip compared with those of the main metabolites.³⁹ To some extent, Lip signals have been considered an annoyance, because they can obscure Lac and alanine; hence, long TE studies are sometimes preferred. No significant difference was found in the maximum LL/Cr-n between the abscess and GBMs in our study. The amino-acid signal intensity may be attributed to the presence of polynuclear leukocytes in the pus samples.^{17–22} The fact that the amino acid metabolites were not detected in the MR spectra from these 8 patients in our study may reflect the low concentration in the pus of the bacteria generating these end products and/or more Lip signals in the abscess cavity.

The sensitivity of DWI and MR spectroscopy for the differentiation of brain abscesses and nonbrain abscesses ranges from 0.72 to 0.96 and 0.86 to 0.96.^{8,15,16} In general, cystic ring-enhancing lesions with hyperintensity on DWI and low ADC values are highly suggestive of brain abscesses; hypointensity on DWI and high ADC values are highly suggestive of necrotic tumors.^{3–7} However, exceptions of DWI studies of both pyogenic brain abscesses and necrotic tumors still exist.^{7,9–16} Single-voxel proton MR spectroscopy is useful as an additional diagnostic technique to distinguish pyogenic brain abscesses from necrotic GBMs.^{17–22} However, aerobic abscesses can simulate intracranial GBMs in single-voxel MR spectroscopy, and

MR spectroscopic imaging is useful in the differentiation as additional diagnostic assistance.

One of the challenges in spectroscopy, even with current automated techniques, is to obtain reliable and reproducible inpatient and outpatient data. To ensure quality control in our data, measurements of Cho-n/Cr-n and Cho-n/NAA-n levels were also measured in the contralateral normal side as part of the MR spectroscopic imaging measurement. Despite possible regional variation in the metabolite ratios within the brain, it was reassuring to find that Cho-n/Cr-n and Cho-n/NAA-n obtained in the GBMs and abscesses were almost identical. Cho-n/Cr-n and Cho-n/NAA-n levels were 1.01 and 0.74 for GBMs and 0.98 and 0.72 for abscesses (Table 1). This not only provides a means for ensuring that the MR spectroscopic data are reliable but also allows for further comparison between the abnormal data and normative data.

It is not always clear what criteria should be used to determine the optimal cutoff values in differentiating GBMs from aerobic abscesses. To obtain potentially useful cutoff values of maximum Cho/Cr, Cho/NAA, and Cho/Cho-n ratios in differentiating GBMs from aerobic abscesses, we chose to minimize the C1 error, which maximizes the average of the observed sensitivity and specificity from the ROC analysis. The sensitivities of maximum Cho/Cho-n (93.3%), Cho/Cr (86.7%), and Cho/NAA (86.7%) ratios in the present study indicate that the metabolite ratios are useful for differentiating between GBMs and aerobic abscesses (Table 2).

This study has several limitations. Because single-voxel MR spectroscopy is limited in voxel size from 1.5 × 1.5 × 1.5 × 2 × 2 × 2 cm, and MR spectroscopic imaging is also limited in voxel size of 1 × 1 × 1 cm, we could not collect meaningful spectra in smaller lesions. In addition, partial volume averaging occurs because some contamination of adjacent perilesional brain tissues or some contamination of the cystic or necrotic portion of GBM and abscess cannot be avoided. In addition, other compounds in abscesses, such as amino acids, and alanine in particular, may affect the spectrum of Lac and Lip. In addition, we used intermediate- and long-TE spectroscopy, because it has been observed that the metabolites in brain abscesses have intermediate-to-long T2 values and are well assigned at TEs of both 272 ms and 136 ms^{20–22}; hence, T2 losses or signal intensity cancellation may mask the Lip signal intensity. The use of short-TE spectroscopy allows for more reliable quantitative determination of Lac, Lip, and macromolecules as markers for hypoxia and necrosis. However, long-echo Cho/Cr provides better discrimination between low-grade astrocytoma and the higher grades than does the short-echo Cho/Cr ratio.³⁴ Last, we focused the study on the common ring-enhancing lesions of GBMs and pyogenic aerobic abscesses. There are other differential diagnostic possibilities of ring-enhancing lesions, such as metastasis, resolving hematoma, and nonpyogenic tubercular and fungal abscesses.

Law et al²⁵ reported that perfusion-weighted and MR spectroscopic imaging may enable distinction between GBMs and metastases. Luthra et al⁴⁰ reported that it may be possible to differentiate among the pyogenic, tubercular, and fungal abscesses based on the morphologic, ADC, and metabolite information.

Conclusion

In conclusion, aerobic abscesses can be differentiated from GBMs by the absence of an elevated Cho peak in the rim-enhancing wall with statistically significant differences compared with normal brain parenchyma. Significant differences were found in the Cho/Cr, Cho/NAA, and Cho/Cho-n ratios in the contrast-enhancing rim between abscess and GBMs. Diagnostic accuracy was mildly higher by Cho/Cho-n ratio than by Cho/Cr and Cho/NAA ratios. An early and correct diagnosis of aerobic abscesses by in vivo MR spectroscopic imaging as a noninvasive method will reduce the high morbidity and mortality rates that occur when diagnosis is delayed.

References

- Lau DW, Klein NC, Cunha BA. Brain abscess mimicking brain tumor. *Heart Lung* 1989;18:634–37
- Mamelak AN, Mampalam TJ, Obana WG, et al. Improved management of multiple brain abscesses: a combined surgical and medical approach. *Neurosurgery* 1995;36:76–86
- Ebisu T, Tanaka C, Umeda M, et al. Discrimination of brain abscess from necrotic or cystic tumors by diffusion-weighted echo planar imaging. *Magn Reson Imaging* 1996;14:1113–16
- Kim YJ, Chang KH, Song IC, et al. Brain abscess and necrotic or cystic brain tumor: discrimination with signal intensity on diffusion-weighted MR imaging. *AJR Am J Roentgenol* 1998;171:1487–90
- Desprechins B, Stadnik T, Koerts G, et al. Use of diffusion-weighted MR imaging in differential diagnosis between intracerebral necrotic tumors and cerebral abscesses. *AJNR Am J Neuroradiol* 1999;20:1252–57
- Noguchi K, Watanabe N, Nagayoshi T, et al. Role of diffusion-weighted echo-planar MRI in distinguishing between brain abscess and tumour: a preliminary report. *Neuroradiology* 1999;41:171–74
- Chang SC, Lai PH, Chen WL, et al. Diffusion-weighted MRI features of brain abscess and cystic or necrotic brain tumors: comparison with conventional MRI. *Clin Imaging* 2002;26:227–36
- Reddy JS, Mishra AM, Behari S, et al. The role of diffusion-weighted imaging in the differential diagnosis of intracranial cystic mass lesions: a report of 147 lesions. *Surg Neurol* 2006;66:246–50; discussion 50–51
- Park SH, Chang KH, Song IC, et al. Diffusion-weighted MRI in cystic or necrotic intracranial lesions. *Neuroradiology* 2000;42:716–21
- Holtas S, Geijer B, Stromblad LG, et al. A ring-enhancing metastasis with central high signal on diffusion-weighted imaging and low apparent diffusion coefficients. *Neuroradiology* 2000;42:824–27
- Tung GA, Evangelista P, Rogg JM, et al. Diffusion-weighted MR imaging of rim-enhancing brain masses: is markedly decreased water diffusion specific for brain abscess? *AJR Am J Roentgenol* 2001;177:709–12
- Hartmann M, Jansen O, Heiland S, et al. Restricted diffusion within ring enhancement is not pathognomonic for brain abscess. *AJNR Am J Neuroradiol* 2001;22:1738–42
- Leuthardt EC, Wippold FJ 2nd, Oswood MC, et al. Diffusion-weighted MR imaging in the preoperative assessment of brain abscesses. *Surg Neurol* 2002;58:395–402
- Nadal Desbarats L, Herlidou S, de Marco G, et al. Differential MRI diagnosis between brain abscesses and necrotic or cystic brain tumors using the apparent diffusion coefficient and normalized diffusion-weighted images. *Magn Reson Imaging* 2003;21:645–50
- Mishra AM, Gupta RK, Jaggi RS, et al. Role of diffusion-weighted imaging and in vivo proton magnetic resonance spectroscopy in the differential diagnosis

- of ring-enhancing intracranial cystic mass lesions. *J Comput Assist Tomogr* 2004;28:540–47
- Lai PH, Hsu SS, Ding SW, et al. Proton magnetic resonance spectroscopy and diffusion-weighted imaging in intracranial cystic mass lesions. *Surg Neurol* 2007;68:S25–36
- Rémy C, Grand S, Lai ES, et al. 1H MRS of human brain abscesses in vivo and in vitro. *Magn Reson Med* 1995;34:508–14
- Dev R, Gupta RK, Poptani H, et al. Role of in vivo proton magnetic resonance spectroscopy in the diagnosis and management of brain abscesses. *Neurosurgery* 1998;42:37–43
- Grand S, Lai ES, Esteve F, et al. In vivo 1H MRS of brain abscesses versus necrotic brain tumors. *Neurology* 1996;47:846–48
- Lai PH, Ho JT, Chen WL, et al. Brain abscess and necrotic brain tumor: discrimination with proton MR spectroscopy and diffusion-weighted imaging. *AJNR Am J Neuroradiol* 2002;23:1369–77
- Garg M, Gupta RK, Husain M, et al. Brain abscesses: etiologic categorization with in vivo proton MR spectroscopy. *Radiology* 2004;230:519–27
- Lai PH, Li KT, Hsu SS, et al. Pyogenic brain abscess: findings from in vivo 1.5-T and 11.7-T in vitro proton MR spectroscopy. *AJNR Am J Neuroradiol* 2005;26:279–88
- Himmelreich U, Dzendrowskyj TE, Bourne R, et al. MR spectroscopy and infectious diseases. *MAGMA* 2000;11:197
- Himmelreich U, Accurso R, Malik R, et al. Identification of Staphylococcus aureus brain abscesses: rat and human studies with 1H MR spectroscopy. *Radiology* 2005;236:261–70
- Law M, Cha S, Knopp EA, et al. High-grade gliomas and solitary metastases: differentiation by using perfusion and proton spectroscopic MR imaging. *Radiology* 2002;222:715–21
- Burger PC, Vogel FS, Green SB, et al. Glioblastoma multiforme and anaplastic astrocytoma. Pathologic criteria and prognostic implications. *Cancer* 1985;56:1106–11
- Britt RH, Enzmann DR, Yeager AS. Neuropathological and computerized tomographic findings in experimental brain abscess. *J Neurosurg* 1981;55:590–603
- Ferreira NP, Otta GM, do Amaral LL, et al. Imaging aspects of pyogenic infections of the central nervous system. *Top Magn Reson Imaging* 2005;16:145–54
- Vigneron DB, Nelson SJ, Murphy-Boesch J, et al. Chemical shift imaging of human brain: axial, sagittal, and coronal P-31 metabolite images. *Radiology* 1990;177:643–49
- Wald LL, Moyher SE, Day MR, et al. Proton spectroscopic imaging of the human brain using phased array detectors. *Magn Reson Med* 1995;34:440–45
- Burtscher IM, Holtas S. In vivo proton MR spectroscopy of untreated and treated brain abscesses. *AJNR Am J Neuroradiol* 1999;20:1049–53
- Li BS, Wang H, Gonen O. Metabolite ratios to assumed stable creatine level may confound the quantification of proton brain MR spectroscopy. *Magn Reson Imaging* 2003;21:923–28
- Dowling C, Bollen AW, Noworolski SM, et al. Preoperative proton MR spectroscopic imaging of brain tumors: correlation with histopathologic analysis of resection specimens. *AJNR Am J Neuroradiol* 2001;22:604–12
- Howe FA, Barton SJ, Cudlip SA, et al. Metabolic profiles of human brain tumors using quantitative in vivo 1H magnetic resonance spectroscopy. *Magn Reson Med* 2003;49:223–32
- Burtscher IM, Skagerberg G, Geijer B, et al. Proton MR spectroscopy and preoperative diagnostic accuracy: an evaluation of intracranial mass lesions characterized by stereotactic biopsy findings. *AJNR Am J Neuroradiol* 2000;21:84–93
- Shimizu H, Kumabe T, Shirane R, et al. Correlation between choline level measured by proton MR spectroscopy and Ki-67 labeling index in gliomas. *AJNR Am J Neuroradiol* 2000;21:659–65
- Kanamori M, Kumabe T, Shimizu H, et al. (201)TI-SPECT, (1)H-MRS, and MIB-1 labeling index of central neurocytomas: three case reports. *Acta Neurochir (Wien)* 2002;144:157–63
- Negendank WG, Sauter R, Brown TR, et al. Proton magnetic resonance spectroscopy in patients with glial tumors: a multicenter study. *J Neurosurg* 1996;84:449–58
- Remin M, Somorjai RL, Deslauriers R, et al. 1H magnetic resonance of human tumors. Analysis of the transverse relaxation of the methylene protons using continuous distributions of relaxation times. *NMR Biomed* 1989;2:142–50
- Luthra G, Parihar A, Nath K, et al. Comparative evaluation of fungal, tubercular, and pyogenic brain abscesses with conventional and diffusion MR imaging and proton MR spectroscopy. *AJNR Am J Neuroradiol* 2007;28:1332–38